

Gas-Phase HO[•]-Initiated Reactions of Elemental Mercury: Kinetics, Product Studies, and Atmospheric Implications

Biswajit Pal and Parisa A. Ariya

Abstract

Mercury is an environmentally volatile toxic fluid metal that is assumed to have a long atmospheric residence time and hence is subject to long-range transport. The speciation and chemical transformation of mercury in the atmosphere strongly influences its bioaccumulation potential in the human food chain as well as its global cycling. To investigate the oxidation of Hg⁰ by HO[•], the dominant daytime atmospheric oxidant, we performed kinetic and product studies over the temperature range 283–353 K under near atmospheric pressure (100 ± 0.13 kPa) in air and N₂ diluents. Experiments were carried out by the relative rate method using five reference molecules and monitored by gas chromatography with mass spectroscopic detection (GC-MS). The HO[•] were generated using UV photolysis of isopropyl nitrite at 300 ≤ λ ≤ 400 nm in the presence of NO. The room-temperature rate constant was found to be (9.0 ± 1.3) × 10⁻¹⁴ cm³ molecule⁻¹ s⁻¹. The temperature dependence of the reaction can be expressed as a simple Arrhenius expression (in unit of 10⁻¹⁴ cm³ molecule⁻¹ s⁻¹) using ethane as the reference molecule: $k_{\text{Hg}^0+\text{HO}} = 3.55 \times 10^{-14} \exp\{(294 \pm 16)/T\}$. The major reaction product, HgO, was identified in the gaseous form, as aerosols and as deposits on the container walls, using chemical ionization mass spectrometry (CI-MS), electron impact mass spectrometry (EI-MS), GC-MS, and cold vapor atomic fluorescence spectrometry (CVAFS). Experimental results reveal that ca. 6% of the reaction products were collected on a 0.2 μm filter as suspended aerosol, ca. 10% were in the gaseous form, and about 80% were deposited on the reaction vessel wall. The potential implications of our results in the understanding of tropospheric mercury transformation are herein discussed.

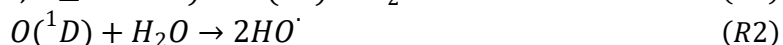
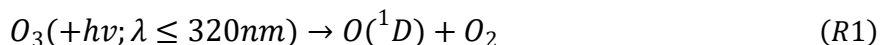
Introduction

Among environmental pollutants, mercury is of particular concern because of its high-biological toxicity ([1](#)), complex biogeochemistry ([2, 3](#)), and relatively long lifetime in the troposphere ([4–6](#)). The U.S. Environmental Protection Agency (EPA) has noted that mercury is a highly dangerous element that persists and cycles in the environment and biota as a result of natural and human activities ([7, 8](#)). The toxicity of mercury is mostly dependent on its chemical form. Methyl mercury is the dominant mercury species in environment and biological materials, and the major known mercury species that is biomagnified ([9](#)). Mercury is introduced into the environment primarily via the atmosphere, which is a significant reservoir of mercury ([10, 11](#)). In the atmosphere, the cycling pathway in the global distribution of mercury proceeds through chemical oxidation/reduction, deposition, and emission from natural and anthropogenic sources ([10](#)).

It has been suggested that about 60–80% of the present mercury emissions to the atmosphere are of anthropogenic origin, with about 50% of anthropogenic mercury entering the global cycle ([12](#)). Recent inventories of global anthropogenic emissions of mercury from 1979 to 1980 to 1995 suggested that there is a substantial reduction in the 1980s and constant emission since then, indicating a concentration increase in the 1980s and a decrease in the 1990s ([13](#)). Total gaseous mercury concentrations in the southern hemisphere are about 1/3 lower than those found in the northern hemispheres with a mean around 1.49 ± 0.11 ([13](#)). Rapid depletion of elemental mercury has been observed in the high-Arctic region (at North America ([14](#)), Greenland ([15](#)), and Svalbard ([16](#))), Arctic ([17, 18](#)), and sub-Arctic ([19](#)) during polar sunrise, with concomitant tropospheric ozone depletion suggesting Hg⁰ oxidation and thus formation of reactive gaseous mercury. Experimental data from a number of studies ([20–24](#)) suggest that the chain reaction leading to ozone depletion in the Arctic is initiated by halogen radicals (Cl[•], Br[•]) through the photolysis of gas-phase halogen compounds. Several researchers have highlighted that BrO and other Br containing radicals are responsible for the oxidation of Hg⁰ and the formation of less volatile Hg^{II} compounds ([17, 25](#)). In this laboratory, we have recently ([26](#)) studied the gas-phase reaction of elemental mercury with atomic (Cl, Br), molecular halogens (Cl₂, Br₂), and BrO ([27, 28](#)) and concluded that based on the presence of the radicals and their kinetics, Br atoms and BrO reactions can explain mercury depletion in the Arctic spring ([14](#)). Interestingly, mercury depletion episodes have also been observed in the Antarctic summer ([29, 30](#)). Recently it has been proposed ([31, 32](#)) that the HO[•] is the dominant atmospheric oxidant apart from the reactive halogen species for Hg⁰ removal in this case, as high HO[•] levels may result from enhanced HONO concentrations due to photodenitrification process in the snowpack ([30](#)).

A limited number of experimental studies have examined the rate of Hg^0 loss in the presence of various oxidants under atmospheric conditions. Some possible reactions of elemental mercury have been investigated with common atmospheric species such as O_3 , HCl , H_2O_2 , and O_2 . The major oxidation pathways of atmospheric Hg^0 are assumed to be the gas-phase reaction with ozone (33–36) and the aqueous oxidation by ozone (37, 38). Hall and Bloom (39) have investigated the reaction of Hg^0 with HCl by performing experiments in darkness and sunlight at different temperatures. The oxidation of Hg^0 by H_2O_2 has been performed by Tokos et al. (40), who suggest that the reaction is thermodynamically favorable. The reaction of Hg^0 with O_2 is unlikely to proceed at a significant rate ($k \leq 1 \times 10^{-23} \text{ cm}^3 \text{ molecule}^{-1} \text{ s}^{-1}$), as Hg^0 was found to be the dominant form of mercury in the ambient atmosphere (41). Some researchers (42–44) have measured the reaction kinetics between various mercury species and free radicals (e.g., HO^\bullet , HO_2^\bullet , and NO_3^\bullet).

HO^\bullet are widely implicated as a major damaging species in free radical pathology (45). They are formed in the aquatic environment by several photolytic pathways, and the dominant source of HO^\bullet in the atmosphere is generally considered to be ozone photolysis followed by reactions with water vapor:

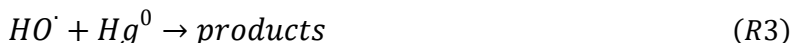


The kinetics of aqueous phase oxidation of Hg^0 by HO^\bullet were determined by Lin and Pehkonen (42) using a steady-state approach to control the HO^\bullet concentration in the presence of excess benzene. In another study (46), the aqueous phase rate constant of $\text{Hg}^0 + \text{HO}^\bullet$ was determined to be $(2.4 \pm 0.3) \times 10^9 \text{ M}^{-1} \text{ s}^{-1}$ using the relative rate technique with methyl mercury as the reference compound, where the reaction proceeds via the molecular Hg^{I} radical which is oxidized to Hg^{II} by dissolved O_2 . There is only limited experimental information available for gas-phase HO^\bullet -initiated reactions of elemental Hg. However, there is a major discrepancy of the reported data for this reaction ranging from 8.7×10^{-14} (at 298 K) to 1.6×10^{-11} (at 343 K) $\text{cm}^3 \text{ molecule}^{-1} \text{ s}^{-1}$ (31, 32, 47), and the reaction products have never been experimentally identified.

The first objective of our present study was to provide kinetic data on the reaction of $\text{Hg}^0 + \text{HO}^\bullet$ at room temperature and over a wide range of temperatures applicable to the atmospheric conditions. Our other objectives included to provide the first experimental product studies of this reaction. Kinetic studies were performed by gas chromatography with mass spectroscopic detection (GC-MS), using a relative rate method over the temperature range 283–353 K under near tropospheric conditions. The reaction products were identified using chemical ionization mass spectrometry (CI-MS), electron impact mass spectrometry (EI-MS), GC-MS, and cold vapor atomic fluorescence spectrometry (CVAFS). The results were employed to assess the direct contribution of the HO^\bullet to the mercury transformation in the troposphere, including mercury depletion in the Arctic boundary layer.

Experimental Section

Relative Rate Kinetic Technique. The relative rate technique was used to determine the rate constant of the HO^\bullet -induced oxidation of elemental Hg. Since this method has already been described several times (26, 36), we only briefly present its principle here. The relative rate coefficients of the Hg^0 - HO^\bullet reaction were determined by comparing their rates of decay with the reference molecules.



If both mercury and reference molecules are removed solely by the reaction with HO^\bullet , and there is no reformation of the reactants, the integrated relative rate equation is expressed as

$$\ln \left\{ \frac{[\text{Hg}^0]_0}{[\text{Hg}^0]_t} \right\} = \frac{k_{\text{Hg}}}{k_{\text{Ref}}} \ln \left\{ \frac{[\text{Ref}]_0}{[\text{Ref}]_t} \right\} \quad (\text{I})$$

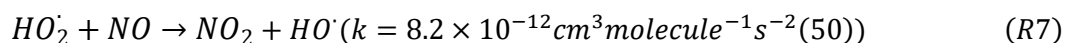
where $[\]_0$ and $[\]_t$ are the corresponding initial concentrations and the concentrations after time t of Hg^0 , and the reference compounds, k_{Hg} and k_{Ref} , are the rate constants for reactions R3 and R4, respectively. A plot of $\ln\{[\text{Hg}^0]_0/[\text{Hg}^0]_t\}$ vs $\ln\{[\text{Ref}]_0/[\text{Ref}]_t\}$ should yield a straight line of slope $k_{\text{Hg}}/k_{\text{Ref}}$ and zero intercept.

The kinetic experiments were performed at near atmospheric pressure (100 ± 0.13 kPa) over the temperature range of 283–353 K in the presence of a reference molecule using isopropyl nitrite as the HO \cdot precursor. A GC-MS was used to determine the rate loss of Hg 0 and the reference compounds upon HO \cdot photolysis.

Experimental Procedures. Kinetic experiments were carried out at atmospheric pressure using thermostated 2 to 5-L double walled reaction chambers equipped with a stopper and double-wall quartz window (2-in. diameter). The outer jacket of the flask was connected to a Neslab RTE 111 circulator, and water was circulated between the walls, which controlled the constant temperature inside the reaction flask during the experiment. Water temperature was held constant to ± 1 K over the temperature range of 283–353 K. A vacuum system was used to prepare the gaseous reactants for all the experiments. Reaction chambers were evacuated to a pressure of ca. 0.013 Pa. Gaseous reactants were transferred to the reaction chamber either using a gastight syringe (Hamilton series 1800 Gastight) or the vacuum system. Liquid reactants were initially injected into a 140 mL reference flask using a microsyringe (Hamilton series). The reference flask, which was held at 6.67–13.3 kPa pressures, connected to the reaction flask and the vacuum system manifold through Teflon valves. Finally, a calculated amount of evaporated liquid substrates (in some cases after dilution into the manifold) were transferred to the reaction chamber from the reference flask. Air or N $_2$ nearly saturated with mercury vapor at 295–298 K was transferred to the reaction flask at approximately 53.3 kPa. The total pressure was then brought to 100 kPa by the addition of N $_2$ or air. To prevent undesired reactions of reagents on the walls of the flask, the reaction chamber was coated with halocarbon wax (Supelco) or covered with dimethyldichlorosilane (DMDCS) (Supelco) (26, 48).

Kinetic studies were carried out using repeated pulse irradiation and sampling into the GC-MS with a gastight syringe. Cyclohexane, *n*-butane, 2-methylpropane, ethane, and cyclopropane were employed as reference compounds since they have known reaction rate constants toward HO \cdot . Experiments were conducted with typical initial concentrations of 0.5–1.0 ppm (part per million volume; 1 ppm = 2.46×10^{13} molecule cm $^{-3}$) for Hg 0 , 2–10 ppm for the reference compounds, 50–100 ppm for isopropyl nitrite, and 5–10 ppm for NO. To ensure the absence of NO $_2$ impurities, NO was passed through a silica gel trap held at -78 °C. NO $_2$ could not be identified outside the instrumental detection limit. The detection limit for NO $_2$ was 6 ppb (parts per billion volume; 1 ppb = 2.46×10^{10} molecule cm $^{-3}$). The diluent gas used was air or nitrogen.

HO \cdot Source and Irradiation technique. HO \cdot were generated by photolysis of isopropyl nitrite (R5–R7) in the presence of air and NO (49). UV–Black lamps (F15T8/BL) were used for photolysis in the range $300 \leq \lambda \leq 400$ nm with a maximum intensity at ~ 365 nm. NO was added to the reaction mixture to convert peroxy radicals to HO \cdot (R7) (49).



Before each kinetic run, the reactants in the reaction chamber were left to homogenize for 20–30 min prior to irradiation. During that time, the reaction chamber was kept in the dark to prevent photolysis of isopropyl nitrite. After homogeneity of the reaction mixture was achieved, photolysis was carried out through a quartz window of the reaction chamber by repeated irradiation technique, where an individual irradiation period ranged from 2 to 5 min long steps of light. Total irradiation times for a particular kinetic study ranged from 20 to 45 min. A digital timer monitored the irradiation time, and an electric fan was positioned inside the photolysis box to maintain a uniform reaction temperature during the irradiation period.

After each irradiation section, the gas samples were injected into the GC-MS using a gastight syringe, and the concentrations of mercury and the reference molecule were monitored. For each run, the volume of the samples injected was 200 μ L. Between each irradiation period, two kinetic runs were monitored by GC-MS as soon as the light was turned off to ensure that no secondary reaction was taking place. We did not observe any evidence for such reactions.

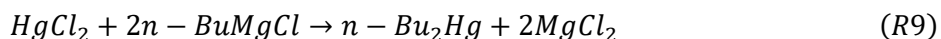
Analytical Procedure for the Kinetic Experiment. Quantitative concentration measurements of mercury and the reference molecules were monitored by MS detection (quadrupole MSD HP 5973) after separation on a gas chromatograph (HP 6890). The GC was equipped with a 0.25 mm i.d. \times 30 m cross-linked phenyl-methyl-

siloxane column (HP 5-MS). The column was operated at a constant flow (1.5 mL min⁻¹) of helium and was kept isothermal at 40 °C for 1 min, after which oven temperature was increased at 25 °C min⁻¹ from 35 to 160 °C. The analysis of the reactant gas mixture of each experiment was monitored initially in the scanning mode of the MSD, and then the corresponding kinetic run was followed by the single ion-monitoring (SIM) mode. The mass spectrometer was set to monitor several masses (*m/z* values) of the reactants and reference compounds. These *m/z* values were selected in an effort to avoid overlaps with each other and with masses of potential transformation products. *m/z* values of 199, 200, 201, and 202 were monitored for mercury in the SIM, and the observed isotopic ratios of the corresponding ions are in good agreement with the results 56:78:44:100, obtained from theoretical calculation. The detection limit of was determined to be 10 ppb. Each compound's retention time was determined by direct injection of that particular compound into the GC.

Analytical Procedure for the Product Analysis. For identification and quantification of the products of the Hg⁰-HO[•] reaction, the pre-concentrated reaction products were collected either in a trap cooled by liquid nitrogen or dissolved in a small volume of solvent and then analyzed by different analytical methods as described below. The other volatile products coming from the photochemical decomposition of the HO[•] source were directly identified by injecting the gaseous sample into the GC-MS, as described in the previous section.

Direct Probe Mass Spectrometry. The collection and analysis of the reaction products was performed in two different ways. In the first, after completion of the reaction, the reaction flask was heated to 363 K, and volatile products were collected by slowly passing the gas mixture using a vacuum system from the reaction chamber through a Pyrex tube (1.1 mm i.d. × 10 cm length) immersed in liquid nitrogen. In the second, the walls of the reaction chamber were washed with 20 mL of 36% HCl, of which 0.4 mL was then transferred to a Pyrex tube (1.1 mm i.d. × 10 cm length). Immediately after collection excess HCl inside the tube was evaporated by slow heating at 90 °C in a water bath. Products collected by these methods were evaporated at stepwise-elevated temperatures from the tube into a chemical and electron impact ion source of a Karatos MS25RFA mass spectrometer using direct probe.

Derivatization. This method is aimed to selectively identify Hg²⁺ in the form of a volatile organomercury compound, *n*-Bu₂Hg, as described in our previous work (36). In the first step, the wall of the reaction flask was treated with 20 mL of 36% HCl, which resulted in the formation of HgCl₂. Excess HCl was evaporated from the sample by slow heating, and it became a white residue. Derivatization of the resulting residue was then carried out according to the procedure reported earlier (51, 52). Two milliliters of toluene and 0.4 mL of 2 M *n*-butylmagnesium chloride in tetrahydrofuran were added to the white residue, and the mixture was centrifuged at 273 K for 10 min with occasional shaking. Subsequently, 0.4 mL of 0.6 M HCl was added to quench the excess derivatizing agent. Finally, the mixture was centrifuged, and the organic phase was collected for analysis by GC-MS.



CV-AFS. For quantitative estimation of the oxidized product in the reaction chamber, reaction samples were prepared by treating the reaction flask walls, Teflon filters (0.22 μm), and coiled Pyrex trap with a mixture of 20 mL of 40% HNO₃ and 0.5 mL of 30% H₂O₂. The samples were diluted to 100 mL and then heated to 350 K for 30 min to decompose H₂O₂. The samples were analyzed with cold vapor atomic fluorescence spectrometer (CV-AFS) (Tekran 2600) using NaBH₄ as a reducing agent. Calibration was accomplished using standard solutions prepared by appropriate dilution from a stock solution of mercuric nitrate. The ionic Hg in the experimental solution was determined after NaBH₄ reduction and then purging of the Hg⁰ to an Au-trap, which led to the CVAFS detector.

Chemicals and Materials. All the chemicals were obtained from commercial sources and were used as supplied. Mercury (99.99% purity), ethane (99%), *n*-butane (99%), 2-methylpropane (99%), cyclopropane (99+%), nitric oxide (98.5%), silica gel, sodium nitrite (99.99%), sodium borohydride (99.99%), and *n*-butylmagnesium chloride (2 M solution in tetrahydrofuran) were purchased from Aldrich Chemical Co., Inc. Cyclohexane (99.7%), toluene (99.9%), hydrogen peroxide (30%), hydrochloric acid (Trace Metal grade), nitric acid (Trace Metal grade), mercuric nitrate (98+%), sodium chloride (99.6%), sodium hydroxide (99%), and sodium sulfate (99.9%) were supplied by Fisher. Sodium bicarbonate (99.7%) was purchased from Merck. Isopropyl alcohol (USP grade) was

received from ACP Chemicals Inc. The UHP nitrogen (certified oxygen content <5 ppmv), Ultrapure air (total hydrocarbons content < 0.1 ppm), and helium were purchased from Matheson. Millipore MQ-water of 18.2 MΩ cm resistance was used throughout the experiment. Isopropyl nitrite used as HO[•] precursor was prepared and purified according to the procedure described below.

Isopropyl alcohol (i-prOH) and sodium nitrite (NaNO₂) in solution were cooled to -5 °C to 0 °C and slowly added to hydrochloric acid, which was maintained at the same temperature. The reaction mixture was maintained at -5 to 0 °C until the reaction was completed. Two phases were separated, the organic phase containing isopropyl nitrite. The final product was washed twice with saturated NaHCO₃ and twice with water and then dried over anhydrous Na₂SO₄. The isopropyl nitrite purity (96%) was verified by MS detection (quadrupole MSD HP 5973) after separation on a gas chromatograph (HP 6890) and stored at 0 °C in the dark.

Results and Discussion

Wall Loss. To see the loss of reactants to the walls and their possible effect on the reaction kinetics, several wall loss experiments were performed, by letting Hg⁰, reference compounds, and isopropyl nitrite stay in the reaction flask during the equilibrium. Blank experiments in a Pyrex flask with nontreated walls revealed that there was a decrease of gas phase concentration immediately after the addition of the reactant gas mixture. To decrease the wall loss of the compounds, the walls of the reaction flask were treated with halocarbon wax or coated with a silylating agent, DMDCS. In addition, the reaction mixture was given sufficient time to equilibrate with the walls before starting the reaction to minimize the effect of adsorption on the reaction kinetics. As reported in our earlier work (26), the rate of adsorption of the substrates on the halocarbon wax coating is less significant in comparison with the DMDCS coating or with noncoated flasks. Halocarbon wax, therefore, was chosen for the kinetic experiments. Wall loss measurements showed that the rate of wall loss of Hg⁰ at 298 K in ca. 0.4 cm⁻¹ surface-to-volume ratio (s/v) is $\sim 2.6 \times 10^{-3} \text{ min}^{-1}$ (where [Hg⁰] = 0.5 ppm). The decrease in concentration is about 4% over the 30 min period immediately after the addition of reactants to the flask and did not exceed 2% over the equilibrium time (2 h). In our experiment, relative rate studies of Hg⁰-HO[•] were mostly performed using cyclopropane as the reference molecule. The rate loss of cyclopropane was estimated to be $(4.6\text{--}5.2) \times 10^{-3} \text{ min}^{-1}$ in the concentration range of 2–10 ppm at 298 K in ca. 0.4 cm⁻¹ s/v ratio. However, the decrease in concentration is $\sim 5\%$ over a 30 min period immediately after the addition of the reactants to the flask and never showed a decrease greater than 2.5% over 2 h time. A similar wall loss trend was observed in the case of ethane, as a reference molecule. In the case of isopropyl nitrite, the rate of wall loss at 298 K in ca. 0.4 cm⁻¹ s/v ratio was $9.3 \times 10^{-3} \text{ min}^{-1}$ (where [isopropyl nitrite] = 50 ppm) with a decrease in concentration of $\sim 7\%$ in 30 min period and did not exceed 4% over the several hours.

TABLE 1. Literature Rate Constants, k_{Ref} , for the Reaction of HO[•] with Reference Compounds Employed in These Studies

compound	k_{Ref} (298 K), cm ³ molecule ⁻¹ s ⁻¹	reference
cyclohexane	$(7.21 \pm 1.44) \times 10^{-12}$	Atkinson (54)
<i>n</i> -butane	$(2.44 \pm 0.35) \times 10^{-12}$	Atkinson (54)
2-methylpropane	$(2.19 \pm 0.26) \times 10^{-12}$	Atkinson (54)
cyclopropane	$(8.40 \pm 0.63) \times 10^{-14}$	Atkinson (54)
	$(6.49 \pm 0.46) \times 10^{-14}$	Clarke et al. (55)
ethane	$(2.54 \pm 0.34) \times 10^{-13}$	Atkinson (54)
	$(2.52 \pm 0.12) \times 10^{-13}$	Clarke et al. (55)

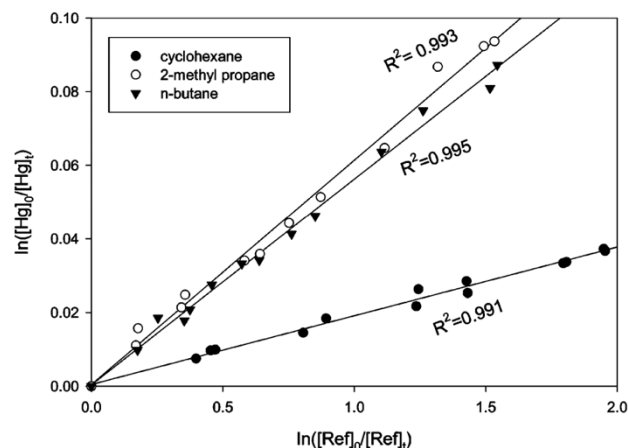


FIGURE 1. Relative rate plots for the reaction of HO[•] with Hg⁰ using cyclohexane, *n*-butane, and 2-methylpropane as reference compounds in air at 298 K.

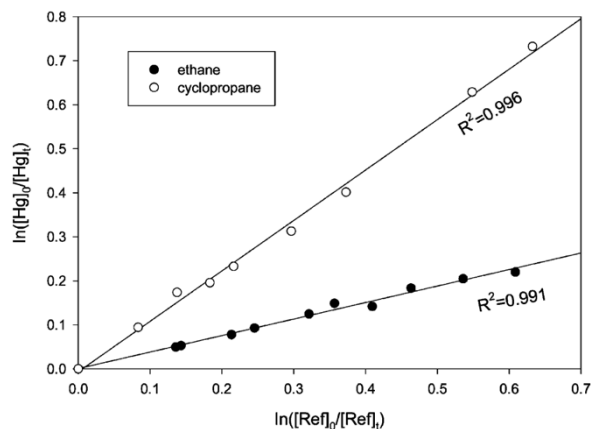


FIGURE 2. Plots of $\ln([Hg]_0/[Hg]_t)$ vs $\ln([Ref]_0/[Ref]_t)$ for the reaction of HO^\bullet with Hg^0 using ethane and cyclopropane as reference compounds in air at 298 K.

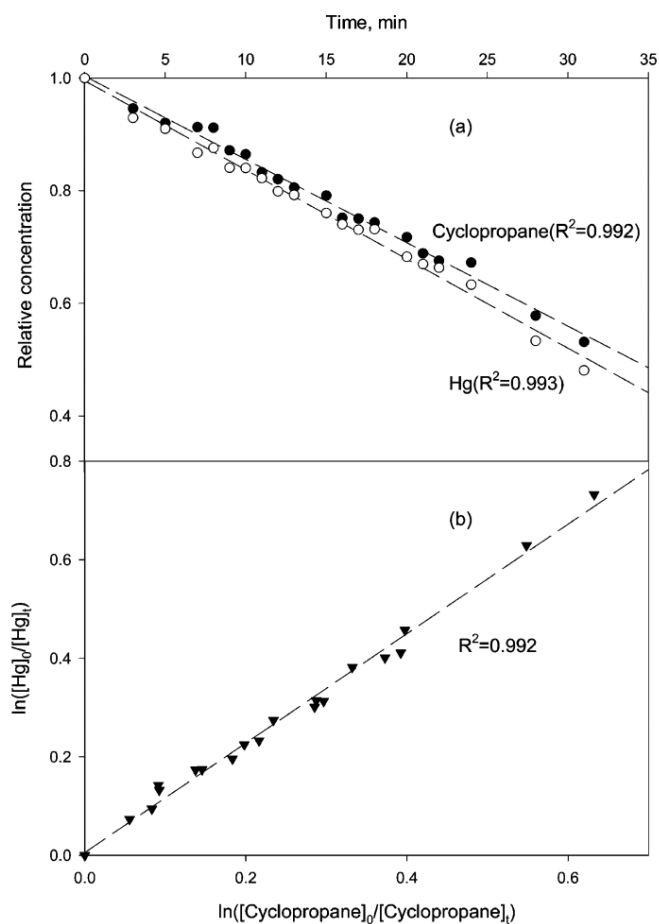


FIGURE 3. (a) Relative concentration of mercury and cyclopropane with different photolysis time at 298 K in air and (b) their corresponding relative rate plot.

Relative Rate Study. Separate experiments were carried out with Hg^0 or an individual reference molecule in air and in nitrogen under photolysis to ensure that no decrease of the GC-MS signal took place in the absence of a HO^\bullet source. Losses of Hg^0 were also insignificant (<5%) in a system containing gaseous mercury in air and in nitrogen

with the reference in the absence of HO[•]. Our targeted experiments showed that there was no observable dark reaction between isopropyl nitrite with Hg⁰ or the reference molecule. Therefore, the loss of mercury and the reference molecule is assumed to be entirely due to reaction with HO[•]. Average concentrations of HO[•] were measured to be $(1.0 \pm 0.5) \times 10^8$ radicals cm⁻³ from the decay rates of *n*-butane and 2-methylpropane. A few experiments were performed by irradiation of the reaction mixture for 5–6 h to verify possible desorption reactions. However, in all cases no increase in the concentration of reactants was observed at any degree of conversion, which nullify the possibilities of desorption reactions. Given the rate constant value of $(2.8 \pm 0.5) \times 10^{-35}$ cm⁶ molecule⁻² s⁻¹ for the Hg⁰-NO₂ reaction (53) in N₂ diluent under experimental conditions this reaction is unlikely to influence our measured data. The most probable gaseous nitrating agent is HNO₃ formed in the reaction HO[•] + NO₂ (+M) → HNO₃ (+M). However, we did not detect HNO₃ in the photooxidation of the Hg⁰-(CH₃)₂CHONO-NO mixture.

TABLE 2. Rate Coefficients of Mercury at 298 K for the HO[•]-Initiated Reactions of Gaseous Mercury Relative to Different Reference Compounds at 101.32 kPa Total Pressure^a

<i>V</i> _{fl} , L	diluent gas	reference	[ref], ppm	<i>k</i> _{Hg} / <i>k</i> _{Ref}	<i>k</i> ^{<i>c</i>} _{Hg+HO} × 10 ¹⁴ cm ³ molecule ⁻¹ s ⁻¹
3	air	cyclohexane	5	0.019 ± 0.002	13.7 ± 1.44
3	air	cyclohexane	10	0.015 ± 0.001	13.0 ± 0.72
3	air	<i>n</i> -butane	6	0.056 ± 0.001	13.6 ± 0.24
3	air	2-methylpropane	5	0.060 ± 0.002	13.1 ± 0.44
3	air	cyclopropane	2	1.114 ± 0.057	9.36 ± 0.48
3	air	cyclopropane	4	1.110 ± 0.028	9.32 ± 0.24
3	air	cyclopropane	6	1.117 ± 0.035	9.38 ± 0.29
3	air	ethane	4	0.374 ± 0.015	9.49 ± 0.38
3	air	ethane	8	0.375 ± 0.019	9.52 ± 0.48
3	N ₂	cyclopropane	6	1.105 ± 0.058	9.28 ± 0.48
3	N ₂	cyclopropane	4	1.102 ± 0.049	9.25 ± 0.41
2	air	ethane ^b	4	0.377 ± 0.018	9.58 ± 0.46
2	air	cyclopropane ^b	4	1.125 ± 0.041	9.45 ± 0.34

^a Initial concentration of mercury was 0.5–1.0 ppm. The reaction flask was coated with halocarbon wax unless stated otherwise. The errors correspond to two least-squares standard deviations ($\pm 2\sigma$).
^b DMDCS coating. ^c Data obtained by Atkinson (54).

TABLE 3. Effect of the Wall of the Reaction Container on the Rate Constants for the Reaction of Mercury with HO[•] Using Ethane and Cyclopropane as References in Air at 298 K^a

reference	<i>V</i> _{fl} , L	[ref], ppm	<i>k</i> _{Hg} / <i>k</i> _{Ref}	<i>k</i> ^{<i>b</i>} _{Hg+HO} × 10 ¹⁴ cm ³ molecule ⁻¹ s ⁻¹
ethane	0.14	8	0.378 ± 0.015	9.60 ± 0.38
	2.00	8	0.376 ± 0.017	9.55 ± 0.43
	3.00	8	0.375 ± 0.019	9.52 ± 0.48
	5.00	8	0.374 ± 0.018	9.50 ± 0.46
cyclopropane	0.14	4	1.123 ± 0.046	9.43 ± 0.38
	2.00	4	1.119 ± 0.061	9.40 ± 0.51
	3.00	4	1.110 ± 0.028	9.32 ± 0.24
	5.00	4	1.115 ± 0.047	9.37 ± 0.39

^a Initial concentration of mercury was 0.5–1.0 ppm. The wall of the reaction container was treated with halocarbon wax. The errors correspond to two least-squares standard deviations ($\pm 2\sigma$). ^b Data obtained by Atkinson (54).

The relative rate technique assumes that both the reactant and the reference compounds are solely removed by the reaction with HO[•]. To verify this assumption we performed a series of control experiments. Five reference molecules were used with different reactivities toward HO[•] ranging from 7.38×10^{-14} to 7.21×10^{-12} cm³ molecule⁻¹ s⁻¹ (54, 55) to obtain a more accurate estimate of the Hg⁰ + HO[•] rate coefficient. The rate coefficient values of the reference compound with HO[•] are given in Table 1 (54, 55).

Plots of some typical kinetic results are displayed in Figures 1 and 2 using cyclopropane and ethane as reference compounds. As depicted in Figures 1 and 2, plots of the relative loss of mercury and reference compound upon reaction led to straight lines with near zero intercepts. Figure 3 illustrates the relative concentration of mercury and cyclopropane of their relative rate plot at different irradiation time. Rate coefficients for the reaction of HO[•] with Hg⁰ were calculated from the rate coefficient ratios, *k*_{Hg}/*k*_{Ref}, using the value of *k*_{Ref} (Table 1). All experimental rate coefficients are shown in Table 2, along with the *k*_{Hg}/*k*_{Ref} ratios. The errors quoted in the kinetic data are twice the

standard deviation arising from the least-squares fits ($\pm 2\sigma$) and do not include an estimate of the error in the reference rate coefficients, k_{Ref} . However, the errors of the final rate coefficient given in the text reflect an estimate of the accumulative uncertainties from the least-squares fits (2–10%), concentration measurements (<5%), instrumental (<10%), and due to adsorption (<8%). Good linearity of relative rate plots was observed for all reference molecules. It is well acknowledged that, in the relative rate technique, the result is more reliable when the rate coefficient of the investigated and reference molecules are of the same magnitude. This may not be the case if cyclohexane, *n*-butane, and 2-methylpropane are used as reference compounds. We thus selected ethane and cyclopropane to better estimate the rate constant value of the $\text{Hg}^0\text{-HO}^\bullet$ reaction, and experiments were performed accordingly. The rate constants for the $\text{Hg}^0\text{-HO}^\bullet$ reaction were estimated to be $(9.32 \pm 0.24) \times 10^{-14}$ and $(9.49 \pm 0.38) \times 10^{-14} \text{ cm}^3 \text{ molecule}^{-1} \text{ s}^{-1}$ ($\pm 2\sigma$) at 298 K using Atkinson's rate constant data (54) for cyclopropane and ethane, respectively. However, rate constant values of $(8.19 \pm 0.21) \times 10^{-14}$ and $(9.37 \pm 0.47) \times 10^{-14} \text{ cm}^3 \text{ molecule}^{-1} \text{ s}^{-1}$ ($\pm 2\sigma$) at 298 K were obtained using Clarke et al.'s data (55) for cyclopropane and ethane. The rate constant obtained using a recommended value for the rate constant for ethane ($k(\text{ethane} + \text{HO}^\bullet) = 2.4 \times 10^{-13} \text{ cm}^3 \text{ molecule}^{-1} \text{ s}^{-1}$ at 298 K) reported by NASA/JPL (50) is $(9.0 \pm 0.4) \times 10^{-14} \text{ cm}^3 \text{ molecule}^{-1} \text{ s}^{-1}$ ($\pm 2\sigma$) at 298 K. The rate constants of the reaction of other reference compounds with HO^\bullet were not reported in the NASA/JPL data set (50). Since the recommended rate constant value of the $\text{HO}^\bullet\text{-ethane}$ reaction from the NASA/JPL data set is obtained by averaging the results of the recent investigations (50), we reported our final kinetic rate coefficients ($(9.0 \pm 1.3) \times 10^{-14} \text{ cm}^3 \text{ molecule}^{-1} \text{ s}^{-1}$ (uncertainty represents accumulative errors) at 298 K) for the $\text{Hg}^0\text{-HO}^\bullet$ reaction calculated from the rate coefficient ratios, $k_{\text{Hg}}/k_{\text{Ethane}}$, using the value of k_{Ethane} from the above-mentioned data. The rate coefficients obtained using ethane and cyclopropane as reference compounds were identical within experimental uncertainties, implying that the results are constant and independent of the reference compound. It was also shown that relative rate constants are independent of change in concentration of the reference compound (Table 2).

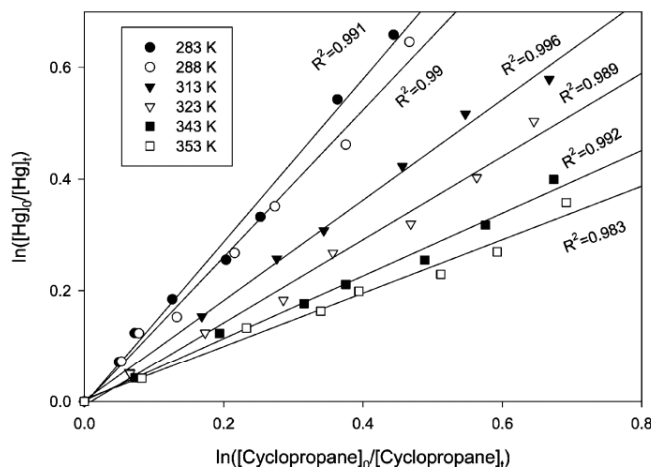


FIGURE 4. Plots of $\ln([\text{Hg}]_0/[\text{Hg}]_t)$ vs $\ln([\text{Cyclopropane}]_0/[\text{Cyclopropane}]_t)$ as a function of temperatures for the reaction of Hg^0 and HO^\bullet using cyclopropane as reference compound in air.

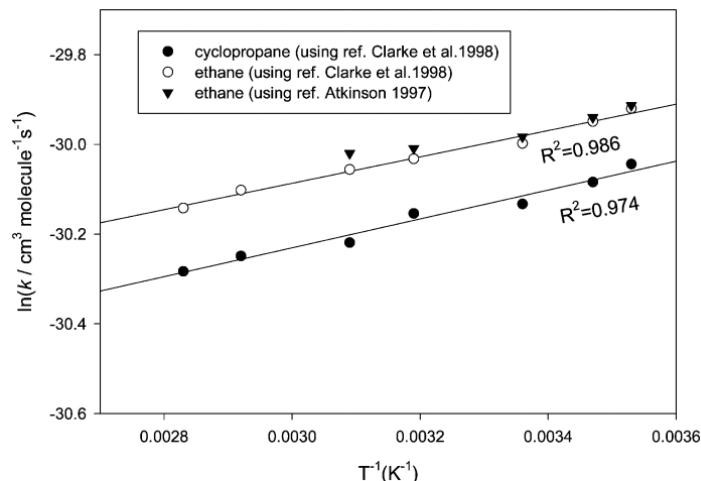


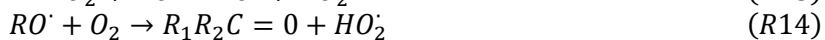
FIGURE 5. Arrhenius plots of kinetic data obtained for the reaction of HO• with Hg⁰ using ethane and cyclopropane as reference compounds in air.

TABLE 4. Absolute Rate Coefficient for the Reaction of HO• with Mercury Using Ethane and Cyclopropane as References as a Function of Temperature and the Associated Arrhenius Parameters^a

reference	temp, K	$k_{\text{Hg}+\text{HO}}^b \times 10^{14} \text{ cm}^3 \text{ molecule}^{-1} \text{ s}^{-1}$	A, $\text{cm}^3 \text{ molecule}^{-1} \text{ s}^{-1}$	E/R
ethane	283	10.1 ± 0.66	3.55×10^{-14}	$-(294 \pm 16)$
	288	9.85 ± 0.53		
	298	9.37 ± 0.47		
	313	9.06 ± 0.47		
	323	8.85 ± 0.49		
	343	8.45 ± 0.67		
	353	8.12 ± 0.24		
cyclopropane	283	8.95 ± 0.35	2.83×10^{-14}	$-(322 \pm 24)$
	288	8.60 ± 0.34		
	298	8.19 ± 0.21		
	313	8.02 ± 0.20		
	323	7.52 ± 0.31		
	343	7.29 ± 0.27		
	353	7.05 ± 0.33		

^a Initial concentration of mercury was 0.5–1.0 ppm. Wall of the reaction container was treated with halocarbon wax. The errors correspond to two least-squares standard deviations ($\pm 2\sigma$). ^b Data obtained by Clarke et al. (55).

It is noteworthy that in the course of the reaction, radicals such as HO• and HO₂• can be generated through secondary reactions, as discussed by Logan et al. (56):



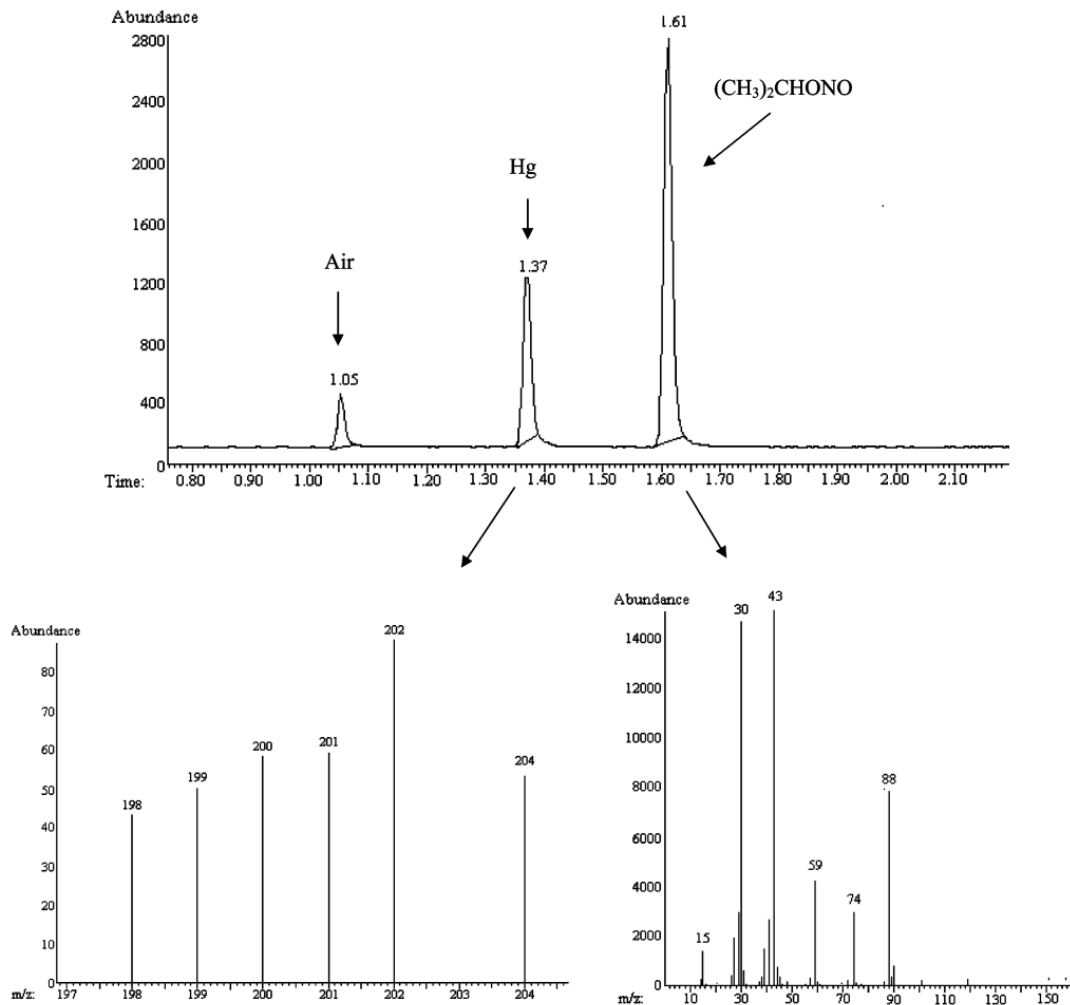


FIGURE 6. Gas chromatogram with mass spectra of the reactant mixture of $\text{Hg}^0\text{-HO}^\bullet$ reaction before irradiation.

In our carrier gas, the oxygen concentration never falls below roughly 10^{15} molecule cm^{-3} . At this oxygen level, alkyl radicals produced by the initial abstraction will react very rapidly to form organo peroxy radicals (RO_2^\bullet). The RO_2^\bullet may in turn react with NO to form organic nitrates or alkoxy radicals, leading to the eventual formation of HO_2^\bullet and RO_2^\bullet , which can complicate the reaction of interest. However, the very good linearity of the plots passing through the origin (shown in Figures 1 and 2) suggests that the secondary reactions are insignificant. Moreover, simple chemical modeling of the above reaction scheme (ACCUCHEM (57)) indicated that the extent of secondary reactions over the course of experiments is negligible.

No substantial differences were observed between the experiments in N_2 and in air (Table 2). We also aged the samples between irradiation to investigate any significant secondary reactions induced by the reaction products; however, we did not observe such phenomena under our experimental conditions.

Preliminary experiments were carried out in order to examine the effect of surface-to-volume ratios (s/v) by performing the reaction in flasks ranging from 0.14 to 5-L (where s/v ratios range from 0.932 to 0.282 cm^{-1}), using ethane and cyclopropane as reference compounds. The results are presented in Table 3, indicating that the relative reaction rates of the compounds of interest were not affected by the different surface-to-volume ratios under experimental conditions, as the $\text{Hg}^0\text{-HO}^\bullet$ reaction proceeds rapidly.

A number of studies have reported (31, 32, 47, 58) a very large discrepancy of the rate constant of the $\text{Hg}^0 + \text{HO}^\bullet$ reaction ranging from 8.7×10^{-14} (at 298 K) to 1.6×10^{-11} (at 343 K) $\text{cm}^3 \text{ molecule}^{-1} \text{ s}^{-1}$. The rate constant value

obtained at 298 K using ethane, $(9.0 \pm 1.3) \times 10^{-14} \text{ cm}^3 \text{ molecule}^{-1} \text{ s}^{-1}$ (uncertainty represents accumulative errors), is in good agreement with that obtained in the work of Sommar et al. ($k = (8.7 \pm 2.8) \times 10^{-14} \text{ cm}^3 \text{ molecule}^{-1} \text{ s}^{-1}$ at 298 K) (31), who also employed a relative rate technique. Bauer et al. (32) have obtained an upper limit for rate coefficient ($1.2 \times 10^{-13} \text{ cm}^3 \text{ molecule}^{-1} \text{ s}^{-1}$) at 298 K using the pulsed laser photolysis-pulsed laser-induced fluorescence (PLP-PLIF) technique under pseudo-first-order condition, which is consistent with our observation error limits. A very recent theoretical paper (58) has calculated a somewhat higher rate constant ($3.2 \times 10^{-13} \text{ cm}^3 \text{ molecule}^{-1} \text{ s}^{-1}$) at 298 K than that determined here. It is noted that the rate coefficient ($1.6 \times 10^{-11} \text{ cm}^3 \text{ molecule}^{-1} \text{ s}^{-1}$ at 343 K) measured by Miller et al. (47) is approximately a factor of 2 larger than that obtained in this study, although the experimental procedures were similar to those in our studies and Sommar et al.'s studies (31).

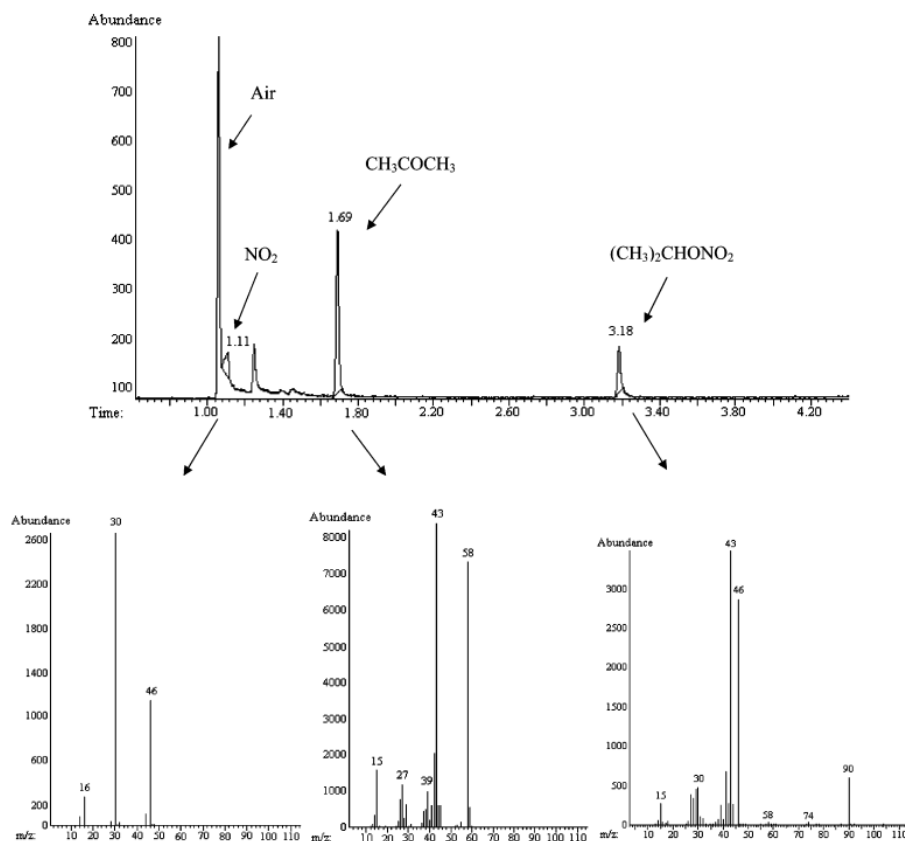


FIGURE 7. Gas chromatogram with mass spectra of the product formed of $\text{Hg}^0_{(g)}\text{-HO}^\bullet$ reaction after 20 min of irradiation.

Temperature Dependence Study. The temperature dependence of the rate coefficients was investigated for the $\text{Hg}^0\text{-HO}^\bullet$ reaction over the temperature range of 283–353 K using ethane and cyclopropane as reference molecules. This study represents the first investigation of the temperature dependence of the reaction of HO^\bullet with elemental mercury at atmospheric pressure. It has been shown (54, 55) that the reaction of HO^\bullet with ethane and cyclopropane exhibits a positive temperature dependence, so we used their corresponding rate constant values over the temperature range of 283–353 K. Figures 4 and 5 show temperature dependence plots. These figures depict that the rate coefficients have small negative temperature dependence. The relative rate constants at different temperatures using ethane and cyclopropane as well as the preexponential factor (A) and activation energy (E) are listed in Table 4. We obtained similar values of preexponential factor (A) and activation energy (E) using cyclopropane and ethane, within the uncertainty limits. Negative temperature dependence is frequently observed for the reaction of organic (59, 60) and inorganic substrates (61–63) with HO^\bullet , especially, when a reaction proceeds via formation of an association complex. This behavior may be expected because the association complex is more readily stabilized at low temperatures (61–63). Analogously, one may expect to observe indications of the equilibrium process $\text{Hg}^0 + \text{HO}^\bullet \rightleftharpoons \text{HgOH}$ in the absence of O_2 . We have attempted to probe HgOH , but we were unable to observe any clear evidence of the existence of stable Hg-OH adducts with a long lifetime ($>\text{min}$) under our experimental conditions. However, due to the potential presence of O_2 in the N_2 system, one cannot rule out the presence of HgOH in a more

controlled environment with the use of a very fast detector. Recently, Bauer et al. (32) suggested the possibility of the reversible reaction as well as the negative temperature dependence of the gas-phase reaction of Hg^0 with HO^\bullet , although it has not been performed experimentally. However, the negative temperature dependency of the same reaction ($k(\text{Hg}^0 + \text{HO}^\bullet \rightarrow \cdot\text{HgOH}, 180\text{--}400 \text{ K}) = 3.2 \times 10^{-13} (T/298 \text{ K})^{-3.06} \text{ cm}^3 \text{ molecule}^{-1} \text{ s}^{-1}$) estimated more recently by Goodsite et al. (58) on the basis of theoretical calculation was due to smaller binding energy of HgOH ($D_0(\text{Hg}\text{--}\text{OH}) = 39.4 \text{ kJ mol}^{-1}$). Similar theoretical data was also reported (58) in the case of $\text{Hg}^0 + \text{Br}$ and $\text{Hg}^0 + \text{I}$ reactions. It is of note that in chemical systems such as HO^\bullet and HI , the negative temperature dependence was related to a temperature-dependent preexponential factor (64). Such reaction appeared to proceed via a low activation barrier due to the low bond energy of $\text{H}\text{--}\text{I}$ and its high polarizability.

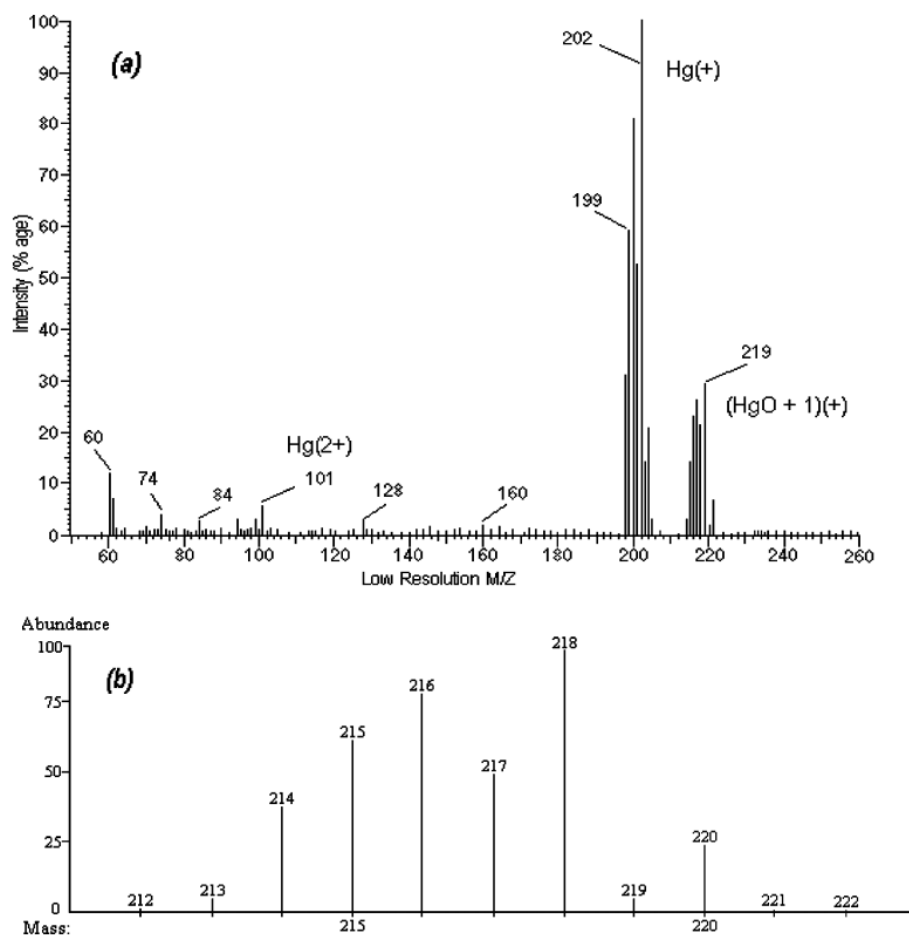


FIGURE 8. (a) Mass spectra of the product formed in the HO -initiated reaction $\text{Hg}^0_{(g)}$ using chemical ionization mass spectrometer and (b) theoretical mass spectra of HgO .

Potential Reactions Mechanism. The most likely reaction path for the oxidation of Hg^0 by the HO^\bullet is the initial formation of $\cdot\text{HgOH}$.



$\cdot\text{HgOH}$ may undergo oxidation via reactions R17, R18, or by R19.



Since $[O_2] \gg [HO^\bullet]$ in the air saturated gas mixture, reaction R17 may dominate over reactions R18 and R19, as is the case in the aqueous phase reaction of Hg^0 with HO^\bullet (46). Under the experimental conditions, we did not identify any other mercury species except HgO , which indeed supports this hypothesis. Moreover, to avoid the oxidative scavenging of *HgOH by oxygen, maintaining $[O_2]$ below $[HO^\bullet]$ would have been required, which was not possible under our experimental conditions. A very recent paper (32) has predicted that the reaction of HO^\bullet with Hg^0 proceeds via a weakly bound intermediate, *HgOH , which subsequently reacts with O_2 , and the overall process is exothermic ($\Delta H = -118 \text{ kJ mol}^{-1}$) with the exothermicity of the individual steps. Based on the ΔG^0_{298} calculation of *HgOH by Stromberg (65), Sommar et al. (31) suggested that the formation of *HgOH by the combination of Hg^0 and HO^\bullet is also slightly exothermic ($\Delta H = \sim -6 \text{ kJ mol}^{-1}$). It can be consequently scavenged by oxygen to produce HgO (R17) due to the low ratio of $p(HO_2^\bullet)/p(O_2)$ in the ambient air, although the reaction R17 is endothermic ($\Delta H = 30 \text{ kJ mol}^{-1}$) (31). In a theoretical study by Goodsite et al. (58), the lifetime of *HgOH was found to be 280 μs , which indeed supports the oxidative scavenging of Hg^I (R17) and is consistent with our experimental observation.

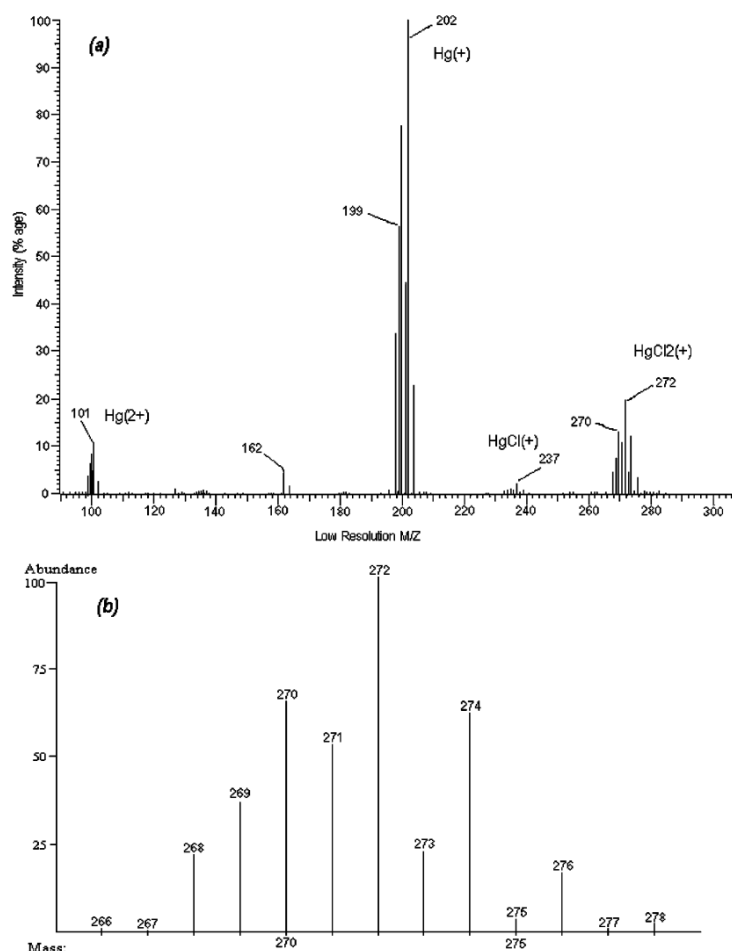


FIGURE 9. (a) Mass spectra of $HgCl_2$ obtained by electron impact mass spectrometer and (b) theoretical mass spectra of $HgCl_2$.

Product Studies. Mechanistic information on the HO^\bullet -initiated oxidation of Hg^0 was obtained from product studies on the photolysis of the $Hg^0-(CH_3)_2CHONO-NO$ mixture under experimental conditions using GC-MS. Typical gas chromatograms with mass spectral data are shown in Figures 6 and 7. Figure 6 corresponds to the composite gas chromatogram with mass spectra of air, Hg^0 , and $(CH_3)_2CHONO$ before irradiation. Air and NO had similar retention times and were often poorly separated. Upon UV irradiation of this sample for 20 min, the formation of the photochemical products NO_2 (R7), CH_3COCH_3 (R6), and $(CH_3)_2CH(ONO_2)$ were observed (Figure 7). One possible source of $(CH_3)_2CH(ONO_2)$ is that the alkoxy radical produced in reaction R5 could react, under high NO_2 concentrations, to also produce isopropyl nitrate, as shown in reaction R20:



Similar observations in various organic reactions have already been reported (e.g., ref 66). Under our experimental conditions, conversion of the reactant Hg^0 to oxidized mercury (R16 and R17) was too low to be identified in GC-MS through syringe sampling. Low vapor pressure of the oxidized mercury and lower sensitivity of the mass spectrometer contributed to the negative detection of the oxidized mercury in the low concentration range. In previous experimental studies by Sommar et al. (31), Bauer et al. (32), and Miller et al. (47), it was suggested that HgO is the only reaction product of the gas phase reaction of the HO^\bullet with elemental mercury. However, this product has not been previously identified experimentally. In this work, we provided evidence for HgO , as a reaction product in the gas phase, from suspended aerosols, and on the wall of the reaction flask, as per three different analytical methods described in the Experimental Section.

In the first method, the chemical structure of the collected gas and aerosol samples in the Pyrex tube were identified by placing it in the direct probe of the MS instrument equipped with a chemical ionization ion source. The probe temperature was elevated to 350 K. In the chemical ionization ion source, NH_3 was used as the reagent gas, so the observed mass spectra of the ion (M^+) should be incremented by one i.e., $(\text{M} + 1)^+$ ion. Therefore, Figure 8(a) represents the mass spectra of HgO , with the m/z ratio of each peak shifted by one. Moreover, the observed isotopic ratio 33.5:56.3:77.4:44.4:100:23 corresponded well with those for the m/z ratios of 214, 215, 216, 217, 218, and 220 of theoretically calculated HgO , as represented in Figure 8(b). The presence of Hg^{2+} on the wall of the reaction flask was confirmed in the form of HgCl_2 , by analyzing the sample using direct MS with an electron impact ion source (Figure 9).

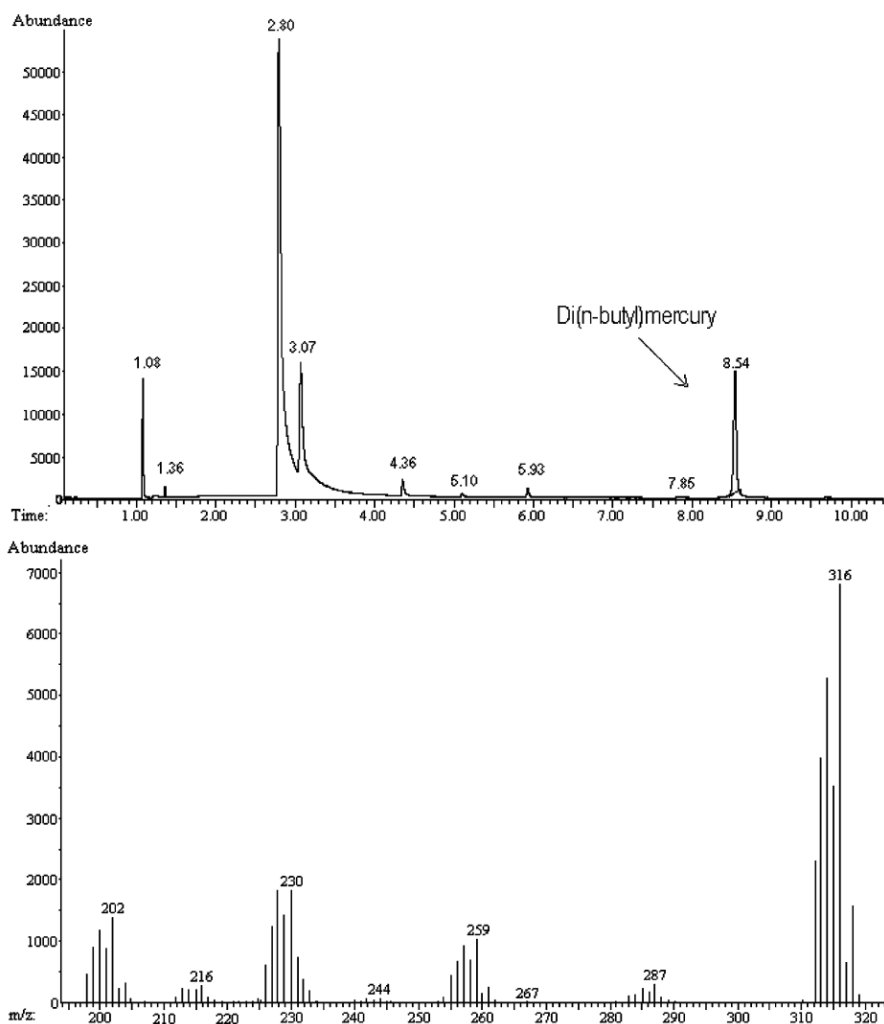


FIGURE 10. Gas chromatogram and the corresponding mass spectra of the derivatized inorganic mercury (di-*n*-butylmercury) eluted at 8.54 min indicating the presence of HgO .

In the second method, reaction products were converted to the more volatile di(*n*-butyl) mercury, as described in the Experimental Section. The derivatized sample was analyzed by GC-MS (Figure 10), which also confirmed the presence of Hg²⁺ (here as HgO) on the wall of the reaction flask.

For quantification of the reaction product from gas, aerosol, and wall deposit, we performed three different sets of CVAFS studies. After completion of the reaction, the reaction flask was evacuated through a 0.22 micron Teflon filter to a residual pressure of ca. 66.7 Pa. The collected sample on the filter was washed with HNO₃/H₂O₂ mixture and analyzed by CVAFS. The result implies that (5.7 ± 1.2)% (number of experiments, *n* = 3, ±2σ) of mercury relative to the amount of Hg⁰ introduced before the reaction was converted into a mercury compound in the aerosol phase. However, in the second set of experiments, the CVAFS analysis of the collected samples from the Pyrex trap after washing with the HNO₃/H₂O₂ mixture recovered (17 ± 2.0)% (*n* = 3, ±2σ) of the mercury that was originally introduced in the gas and aerosol phases. Thus, the amount of mercury recovered in the gas phase is the difference of (5.7 ± 1.2)% and (17 ± 2.0)%, which is (11.3 ± 2.3)% (uncertainty represents weighted cumulative errors). Similarly, in the final set, the walls of the reaction flask were treated with HNO₃/H₂O₂ mixture, collected, and analyzed in CVAFS. Recovery of mercury on the reaction wall was (83 ± 2.1)% (*n* = 3, ±2σ). However, the adsorption of Hg⁰ on halocarbon wax coating was about (4.5 ± 1.4)% (*n* = 3, ±2σ), as described in the wall section. Hence, the recovery of mercury from the wall was (78.5 ± 2.5)% (uncertainty represents weighed cumulative errors), obtained by subtraction of (4.5 ± 1.4)% from (83 ± 2.1)%. Considering all the CVAFS studies, we conclude that the majority of reaction products were deposited on the reaction container wall, although there was a significant amount of reaction products in the gas-aerosol phase.

We have studied the kinetics and products of Hg⁰-HO[•] reaction in nitrogen and in air under the temperature range 283–253 K at near tropospheric pressure. For the first time, we have positively identified HgO as the reaction product in the gas, aerosol, and wall deposits and provided temperature dependence for the kinetics of HO[•]-initiated oxidation of Hg⁰. The room-temperature kinetic part of our work confirms a previous study (32, 57) and is in contrast with other studies (47). Hence, assuming a typical daily tropospheric HO[•] concentration of 1 × 10⁶ radicals cm⁻³ (67), the tropospheric lifetime of mercury against reaction with HO[•] was calculated to be 124 days using the measured rate constant at 298 K. This calculated lifetime hints to the importance of HO[•] as an effective oxidant of tropospheric mercury. However it suggests that observed rapid Arctic mercury depletion cannot be explained by HO[•] chemistry (68).

Author Information

Authors

Biswajit Pal - Departments of Chemistry and Atmospheric and Oceanic Sciences, McGill University, 801 Sherbrooke Street West, Montreal, Quebec H3A 2K6, Canada

Parisa A. Ariya - Departments of Chemistry and Atmospheric and Oceanic Sciences, McGill University, 801 Sherbrooke Street West, Montreal, Quebec H3A 2K6, Canada

Acknowledgment

We cordially thank the Natural Science and Engineering Research Council of Canada (NSERC), the Fond pour la Formation de Chercheurs et l'Aide à la Recherche (FCAR), the Canadian Foundation for Innovation (CFI), the COMERN project, and Environment Canada for financial support as well as Ed Hudson, Clare Salustro, and Jackie Johnstone for proofreading this manuscript.

- (1) Clevenger, W. L.; Smith, B. W.; Winfordner, J. D. *Crit. Rev. Anal. Chem.* **1997**, *27*, 1–27.
- (2) *Environmental Health Criteria for Methyl Mercury*. International Programme on Chemical Safety; World Health Organization (WHO): Geneva, 1990.
- (3) Yan, X.; Yin, X.; Jiang, D.; He, X. *Anal. Chem.* **2003**, *75*, 1726–1732.
- (4) Seiler, W.; Eberling, C.; Slemr, F. *Pageoph* **1980**, *118*, 963–973.
- (5) Slemr, F.; Schuster, G.; Seiler, W. *J. Atmos. Chem.* **1985**, *3*, 407–434.
- (6) Lindqvist, O.; Rodhe, H. *Tellus* **1985**, *37B*, 136–159.
- (7) Sánchez Urfa, J. E.; Sanz-Medel, A. *Talanta* **1998**, *47*, 509–524.
- (8) Walcek, C.; De Santis, S.; Gentile, T. *Environ. Pollut.* **2003**, *123*, 375–381.
- (9) Surma-Aho, K.; Paasivirta, J.; Rekolainen, S.; Verta, M. *Chemosphere* **1986**, *15*, 353–372.
- (10) Schroeder, W. H.; Munthe, J. *Atmos. Environ.* **1998**, *29*, 809–822.

- (11) Bindler, R. *Environ. Sci. Technol.* **2003**, *37*, 40–46.
- (12) Slemer, F.; Brunke, E.-G.; Ebinghaus, R.; Temme, C.; Munte, J.; Wangberg, I.; Schroeder, W.; Steffen, A.; Berg, T. *Geophys. Res. Lett.* **2003**, *30*, 1516–1520.
- (13) Laurier, F. J. G.; Mason, R. P.; Whalin, L.; Kato, S. *J. Geophys. Res.* **2003**, *108*(D17), 4529–4541.
- (14) Schroeder, W. H.; Anlauf, K. G.; Barrie, L. A.; Lu, J. Y.; Steffen, A.; Schneeberger, D. R.; Berg, T. *Nature* **1998**, *394*, 331–332.
- (15) Skov, H.; Christensen, J.; Goodsite, M.; Heidam, N. Z.; Jensen, B.; Wahlin, P.; Geernaert, G. *Environ. Sci. Technol.* **2004**, *38*, 2373–2382.
- (16) Berg, T.; Sekkesaeter, S.; Steinnes, E.; Valdøl, A.-K.; Wibetoe, G. *Sci. Total Environ.* **2003**, *304*, 43–51.
- (17) Linberg, S. E.; Brooks, S.; Lin, C.-J.; Scott, K. J.; Landis, M. S.; Stevens, R. K.; Goodsite, M.; Richter, A. *Environ. Sci. Technol.* **2002**, *36*, 1245–1256.
- (18) Lu, J. Y.; Schroeder, W. H.; Barrie, L. A.; Steffen, A.; Welch, H. E.; Martin, K.; Lockhart, L.; Hunt, R. V.; Boila, G.; Richter, A. *Geophys. Res. Lett.* **2001**, *28*, 3219–3222.
- (19) Poissant, L. 2001, personal communication.
- (20) Barrie, L. A.; Bottenheim, J. W.; Crutzen, P. J.; Rasmussen, R. A. *Nature* **1988**, *334*, 138–141.
- (21) Foster, K. L.; Plastringe, R. A.; Bottenheim, J. W.; Shepson, P. B.; Finlayson-Pitts, B. J.; Spicer, C. W. *Science* **2001**, *291*, 471–474.
- (22) Finlayson-Pitts, B. J.; Livingston, F. E.; Berko, H. N. *Nature* **1990**, *343*, 622–625.
- (23) Bottenheim, J. W.; Fuentes, J. D.; Tarasick, D. W.; Anlauf, K. G. *Atmos. Environ.* **2002**, *36*, 2535–2544.
- (24) Spicer, C. W.; Plastringe, R. A.; Foster, K. L.; Finlayson-Pitts, J.; Bottenheim, J. W.; Grannas, A. M.; Shepson, P. B. *Atmos. Environ.* **2002**, *36*, 2721–2731.
- (25) Boudries, H.; Bottenheim, J. W. *Geophys. Res. Lett.* **2000**, *27*, 517–520.
- (26) Ariya, P. A.; Khalizov, A.; Gidas, A. *J. Phys. Chem.* **2002**, *106*, 7310–7320.
- (27) Raofie, F.; Ariya, P. A. *J. Phys. Chem. A* **2003**, *107*, 1119–1121.
- (28) Raofie, F.; Ariya, P. A. A Product Study of the Gas-phase BrO-initiated Oxidation of Hg⁰: Evidence for Stable Hg⁺ Compounds. *Environ. Sci. Technol.* **2004**, *38* (16), 4319–4326.
- (29) Ebinghaus, R.; Kock, H. H.; Temme, C.; Einax, J. W.; Lowe, A. G.; Richter, A.; Burrows, J. P.; Schroeder, W. H. *Environ. Sci. Technol.* **2002**, *36*, 1238–1244.
- (30) Temme, C.; Einax, J. W.; Ebinghaus, R.; Schroeder, W. H. *Environ. Sci. Technol.* **2003**, *37*, 22–31.
- (31) Sommar, J.; Gårdfeldt, K.; Stromberg, D.; Feng, X. *Atmos. Environ.* **2001**, *35*, 3049–3054.
- (32) Bauer, D.; D’Ottone, L.; Cam puzano-Jost, P.; Hynes, A. J. *J. Photochem. Photobiol. A: Chem.* **2003**, *157*, 247–256.
- (33) Hall, B. *Water, Air, Soil Pollut.* **1995**, *80*, 301–315.
- (34) P’yankov, V. A. *Zh. Obshch. Khim. (Russ. J. Gen. Chem.)* **1949**, *19*, 224–229.
- (35) Biswajit, P.; Parisa, A. A. *J. Phys. Chem. A* **2003**, *107*, 189–192.
- (36) Pal, B.; Ariya, P. A. *Phys. Chem. Chem. Phys.* **2004**, *6*(3), 572–579.
- (37) Iverfeldt, Å.; Lindqvist, O. *Atmos. Environ.* **1986**, *20*(8), 1567–1573.
- (38) Munthe, J. *Atmos. Environ.* **1992**, *26A*, 1461–1468.
- (39) Hall, B.; Bloom, N. S. *Annual Report to the Electric Power Research Institute*; Palo Alto, CA, 1993.
- (40) Tokos, J. J.; Hall, B.; Calhoun, J. A.; Prestbo, E. M. *Atmos. Environ.* **1998**, *32*, 823–827.
- (41) Hall, B. Ph.D. Dissertation, Chalmers University of Technology, Göteborg, University of Göteborg, Sweden, 1992.
- (42) Lin, C.-J.; Pehkonen, S. O. *Atmos. Environ.* **1997**, *31*, 4125–4137.
- (43) Pehkonen, S. O.; Lin, C.-J. *J. AWMA* **1998**, *48*, 144–150.
- (44) Sommar, J.; Hallqvist, M.; Ljungström, E.; Lindqvist, O. *J. Atmos. Chem.* **1997**, *27*, 23–247.
- (45) Ward, P. A.; Till, G. O.; Kunkel, R.; Beauchamp, C. *J. Clin. Invest.* **1983**, *72*, 789–801.
- (46) Gårdfeldt, K.; Sommar, J.; Stromberg, D.; Feng, X. *Atmos. Environ.* **2001**, *35*, 3039–3047.
- (47) Miller, G. C.; Quashnick, J.; Hebert, V. *Abstr. Pap. – Am. Chem. Soc.* **2001**, *221st*, AGRO-016.
- (48) Coquet, S.; Ariya, P. A. *Int. J. Chem. Kinet.* **2000**, *32*, 478–484.
- (49) O’Brien, J. M.; Czuba, E.; Hastie, D. R.; Francisco, J. S.; Shepson, P. B. *J. Phys. Chem.* **1988**, *92*, 18903–18908.
- (50) Chemical Kinetics and Photochemical Data for use in Atmospheric Studies, NASA/JPL Data Evaluation, Jet Propulsion Laboratory, California Institute of Technology, <http://jpldataeval.jpl.nasa.gov> 2003.
- (51) Bulska, E.; Emteborg, H.; Baxter, D. C.; Frech, W.; Ellingsen, D.; Thomassen, Y. *Analyst (London)* **1992**, *117*, 657–663.
- (52) Snell, J.; Qian, J.; Johansson, M.; Smit, K. *Analyst (Cambridge, U.K.)* **1998**, *123*, 905–909.
- (53) Hall, B.; Schager, P.; Ljungström, E. *Water, Air, Soil Pollut.* **1995**, *81*, 121–134.
- (54) Atkinson, R. *J. Phys. Chem. Ref. Data* **1997**, *26*(2), 215–219.
- (55) Clarke, J. S.; Kroll, J. H.; Donahue, N. M.; Anderson, J. G. *J. Phys. Chem. A* **1998**, *102*, 9847–9857.
- (56) Logan, J. A. *J. Geophys. Res.* **1985**, *90*, 10463–10482.
- (57) Braun, W.; Heron, J. T.; Kahaner, D. K. *Int. J. Chem. Kinet.* **1988**, *20*, 51–62.
- (58) Goodsite, M. E.; Plane, J. M. C.; Skov, H. *Environ. Sci. Technol.* **2004**, *38*, 1772–1776.
- (59) Alvarez-Idaboy, J. R.; Mora-Diez, N.; Vivier-Bunge, A. *J. Am. Chem. Soc.* **2000**, *122*, 3715–3720.
- (60) Moriarty, J.; Sidebottom, H.; Wenger, J.; Mellouki, A.; Bras, G. L.

- J. Phys. Chem.* **2003**, *107*, 1499–1505.
- (61) Hynes, A. J.; Wine, P. H.; Nicovich, J. M. *J. Phys. Chem.* **1988**, *92*, 3846–3852.
- (62) Jones, B. M. R.; Burrows, J. P.; Cox, R. A.; Penkett, S. A. *Chem. Phys. Lett.* **1982**, *88*, 372–376.
- (63) Williams, M. B.; Camuzano-Jost, P.; Bauer, D.; Hynes, A. J. *Chem. Phys. Lett.* **2001**, *344*, 61–67.
- (64) Camuzano-Jost, P.; Crowley, J. N. *J. Phys. Chem.* **1999**, *103*, 2712–2719.
- (65) Stroemberg, D. Some mercury compounds studied by relativistic quantum chemical methods. Ph.D. Thesis, Göteborg University and Chalmers University of Technology, 1990.
- (66) Arey, J.; Aschmann, S. M.; Kwok, E. S. C.; Atkinson, R. *J. Phys. Chem.* **2001**, *105*, 1020–1027.
- (67) Prinn, R. G.; Weiss, R. F.; Miller, B. R.; Huang, F. N.; Alyea, J.; Cunnold, D. M.; Frasar, P. G.; Hartley, D. E.; Simmonds, P. G. *Science* **1995**, *269*, 187.
- (68) Ariya, P. A.; Dastoor, A. P.; Amyot, M.; Schroeder, W. H.; Barrie, L.; Anlauf, K.; Raofie, F.; Ryzhkov, A.; Davignon, D.; Lalonde, J.; Steffen, A. *Tellus, Ser. B*, **2004**, 1–7.

<https://pubs.acs.org/doi/full/10.1021/es0494353>